Scientia Iranica B (2023) 30(4), 1265–1278

Sharif University of Technology
Scientia Iranica
Transactions B: Mechanical Engineering
http://scientiairanica.sharif.edu

Research Note

Vibration behavior of misaligned rotor with the asymmetric shaft using Timoshenko beam theory

H. Jamshidi[a], A.A. Jafari[b,c,*], and P. Jamshidi[d]

a. *Faculty Member of Mechanical Engineering, Parand Branch, Islamic Azad University, Tehran, Iran.*
b. *Faculty Member of Mechanical Engineering, West Tehran Branch, Islamic Azad University, Tehran, Iran.*
c. *Faculty Member of Mechanical Engineering, K.N. Toosi University of Technology, Tehran, Iran.*
d. *Head of Turbo Compressor Maintenance Department at SPGC, Tehran, Iran.*

Received 15 March 2021; received in revised form 6 November 2021; accepted 19 December 2022

KEYWORDS
Asymmetric rotor;
Timoshenko beam theory;
Misalignment;
Mass unbalance;
Vibration.

Abstract. In the present study, an accurate model is used for analyzing an asymmetric shaft with misalignment and under unbalance forces in rotating coordinates verified by developing an experimental test. The asymmetric rotor is modeled by the Timoshenko beam theory. The differential equations of motion are discretized by Rayleigh-Ritz method and derived from Hamilton's principle. Thereafter, according to the results, a frequency range is detected in which resonance and instability will occur. The dynamic behavior of the rotor is investigated near the boundary of the instability region. Various parameters including unbalance and misalignment induced forces, and the dimensions of the shaft are taken into account. Finally, vibration responses of the system and their Fast Fourier Transform (FFT) are presented graphically to determine the frequencies of the harmonic responses. It is concluded that the asymmetry of the shaft and misalignment fault severely affect the dynamic response of the rotor. Moreover, the accuracy of the results is increased by applying the Timoshenko beam theory. By developing an experimental test for the rotor system with misalignment fault, this model has been carefully verified. The experimental results obviously obtained the unstable operating area as acquired by the differential equations of motion.

1. Introduction

With the growing demand for a proper analytical approach to rotor systems, which is very important in the design, identification, and control of such systems, the need for presenting more reliable mathematical models in rotor dynamics is felt more than ever [1]. In the case of a high-speed rotor with a thick shaft, it is important to understand the dynamic behavior of the system experiencing misalignment and mass unbalance excitations [2]. There are several factors that give rise to the misalignment of a rotor system and they include differential thermal increase, asymmetry of applied loads, and unequal base settlement [3]. A number of studies have addressed the problem of modeling rotors under misalignment forces. However, an analytical model that properly addresses the dynamic behavior of an asymmetric rotor with the help of Timoshenko beam model under the impact of unbalance and misalignment is still highly on demand. Gibbons [4] presented a model for deriving the reaction forces and moments generated from misaligned couplings, as shown in Figure A.1. An experimental study of the effect

*. *Corresponding author.*
E-mail address: ajafari@kntu.ac.ir (A.A. Jafari)

doi: 10.24200/sci.2022.57914.5473

of misalignment on cylindrical and three-lobe journal bearings was carried out by Prabhu [5]. Ganesan and Padmanabhan [6] considered two shafts with flexible coupling under parallel misalignment forces. The response of the system under the effect of parametric excitations has been determined and their effects are quite clear at $\frac{1}{2}$, $\frac{1}{3}$, and $\frac{1}{4}$ of the principal parametric resonance. Wan et al. [7] analyzed theoretically and experimentally the dynamic behavior of a multi-disk rotor under the misalignment force and the nonlinear oil film force in bearings. In the frequency response, the frequencies of 2X, 3X, 4X were detected due to the misalignment coupling. Redmond and Al-Hussain and Redmond [8] and Al-Hussain [9] studied the lateral and torsional behavior of two shafts with parallel misalignment coupling. Hujare and Karnik [10] analyzed the aluminum shaft rotor system with parallel misalignment coupling using Finite Element Analysis (FEA). Verma et al. [11] experimentally investigated effects of misalignment on rotor shaft vibration and stator current signature. Ma et al. [12] analyzed the instability of an overhung rotor under parallel and angular misalignment forces in the run-up and run-down periods. Jalan and Mohanty [13] identified the effect of misalignment and unbalance on the response of a rotor system experimentally by using a model-based method. They demonstrated 2X vibration response as the misalignment result. Sudhakar and Sekhar [14] summarized different findings on coupling misalignment modeling. As shown in previous studies, the characteristics of a rotor with a misalignment defect can be detected in vibration magnitude at a speed of 2X in Fast Fourier Transform (FFT) analysis. Wang and Jiang [15] investigated the vibration features of a dual rotor with unbalance and misaligned coupling numerically and experimentally. Gao et al. [16] investigated the vibration response of a rotor-bearing system under misalignment forces and Integral Squeeze Film Damper (ISFD). Wang and Gong [17] analyzed the dynamic behavior of coupling misalignment between two rotors. In the case of rotors with asymmetric shafts, Tondl [18] investigated the dynamic behavior of these shafts with different stiffness levels and presented the boundaries of instability. Also, Badlani and Kleinhenz and Hsiao [19] analyzed the stability of this asymmetric rotor by modeling it. Srinath et al. [20] investigated the instability of an asymmetric rotor. He utilized a complex model that consisted of higher degrees of freedom. Hili et al. [21] studied the stability and dynamic behavior of an unbalanced and asymmetric rotor to indicate the effect of dynamic features of Active Magnetic Bearings (AMBs). Raffa and Vatta [22] derived differential equations of motion for an asymmetric shaft using Timoshenko beam theory. Jafari and Jamshidi [23] analyzed the dynamic response of a rotor with an asymmetric shaft subject to unbalance and misalignment forces. They extracted differential equations of motion using the Euler-Bernoulli theory, considering the effect of high-order large deformations. Shahgholi and Khadem [24] studied the stability of a steady-state response of the asymmetric shaft by considering the effects of dissimilar mass moment of inertia. They used the method of multiple scales.

Feng et al. [25] investigated the vibration behavior of an asymmetric rotor under misalignment force. They observed that maximum amplitude occurred near half of the natural frequency $\frac{\omega_n}{2}$ as a result of asymmetry in the shaft, while the dominant frequency could be seen near ω_n when subjected to parallel misalignment. Li et al. [26] studied the nonlinear vibration behavior of the asymmetric rotor with parallel misalignment between two rotors. The responses showed that the super-synchronous component in the frequency of 2X was important to identify and diagnose misalignment of the rotor. Rahi [27] employed the improved couple stress theory to investigate the effect of size on dynamic response in a micro drill, which is under the effect of mounted mass at its free end. Farshidianfar and Soheyli [28] analyzed the impact of shaft rotation on its natural frequency. After deriving the equation of motion, it was solved by using the new analytical method. Wang and Zhu [29] introduced a new model for analyzing a rotor bearing system using rolling element bearings. Filippi and Carrera [30] employed high-order finite beam elements to investigate the stability and transient response of unsymmetric rotors. They analyzed the impact of angular acceleration on the response of a realistic gas turbine under anisotropic bearings. Jamshidi and Jafari [31,32] studied accurate models using asymmetric shaft with misalignment and under unbalance forces in rotating coordinates verified by developing an experimental test. They also utilized Timoshenko theory to improve the accuracy of the results.

Bab et al. [33] investigated dynamic stability and nonlinear vibration analysis of a rotor system with flexible/rigid blades. They improved the method using numerical method. Lu et al. [34] modeled coupling of rotors as a cantilever dual-rotor system for the first time. The proposed method in this study can provide guidance for analyzing coupling of rotors. In some studies, the vibration behavior of a rotor under misalignment forces is investigated by modeling the asymmetric shaft as the Euler-Bernoulli beam model. Other researchers have previously focused on deriving differential equations of motion for a rotor with an asymmetric Timoshenko shaft in rotating coordinates. However, these studies did not include modeling misalignment forces or considering their effects on the dynamic behavior of the rotor.

The present study aims to develop a model for a rotor with an asymmetric Timoshenko shaft, taking into consideration the effects of mass unbalance and misalignment induced forces on the dynamic behavior of the rotor. Effects of parameters such as the dimensions of the cross-section of the shaft, mass moment of inertia, and unbalance and misalignment forces are considered. In order to derive the differential equations of motion for this system, Hamilton's principle is used and then, the coupled equations are solved through the numerical method. Finally, Campbell curves are plotted for two shafts with different cross-sections. According to the obtained equations and results, one can predict the impacts of shaft asymmetry and mass unbalance induced force on the dynamic response of the rotor system.

2. The dynamic model and differential equations of motion

Figure 1 represents a model of a flexible rotor connected to an electric motor through coupling. This rotor consists of a disk mounted at distance L_1 from bearing number 2. The cross-section of the shaft is rectangular with length L. The mass of the disk is denoted by M_D and is assumed to be rigid with radius R_D.

The displacements of the rotating shaft are denoted by $u(z,t)$, $v(z,t)$, and $w(z,t)$, where these variables refer to the deflection of the shaft in an arbitrary location z in the x, y, and z directions, respectively. Misalignment is shown in Figure A.1.

The transformation between the inertial coordinate $x_0 - y_0 - z_0$ and the rotating coordinate $x - y - z$ is described by Euler angles $\phi(z,t)$, $\theta(z,t)$, and $\Psi(t)$, as shown in Figure 2.

The angular velocities of the rotating shaft can be obtained by the Euler angles. The angular velocities can be derived as [3]:

$$\vec{\omega} = \dot{\psi} e_{z_0} + \dot{\theta} e_{y_1} + \dot{\phi} e_{x_2} = R_\phi . R_\theta . \dot{\psi}(\vec{k}) + R_\phi . \dot{\theta}(\vec{j})$$

$$+\dot{\phi}(\vec{i}) = \begin{bmatrix} 1 & 0 & 0 \\ 0 & \cos\phi & \sin\phi \\ 0 & -\sin\phi & \cos\phi \end{bmatrix}$$

$$\begin{bmatrix} \cos\theta & 0 & -\sin\theta \\ 0 & 1 & 0 \\ \sin\theta & 0 & \cos\theta \end{bmatrix} \begin{bmatrix} 0 \\ 0 \\ \dot{\psi} \end{bmatrix}$$

$$+ \begin{bmatrix} 1 & 0 & 0 \\ 0 & \cos\phi & \sin\phi \\ 0 & -\sin\phi & \cos\phi \end{bmatrix} \begin{bmatrix} 0 \\ \dot{\theta} \\ 0 \end{bmatrix} + \begin{bmatrix} \dot{\phi} \\ 0 \\ 0 \end{bmatrix}, \quad (1)$$

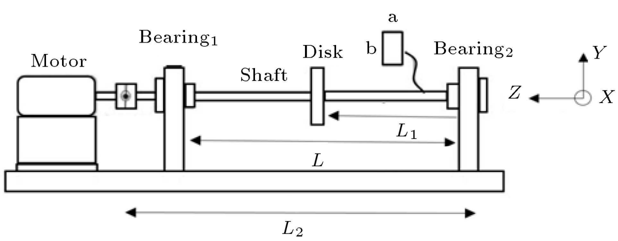

Figure 1. Flexible rotor system with a rectangular cross-section shaft.

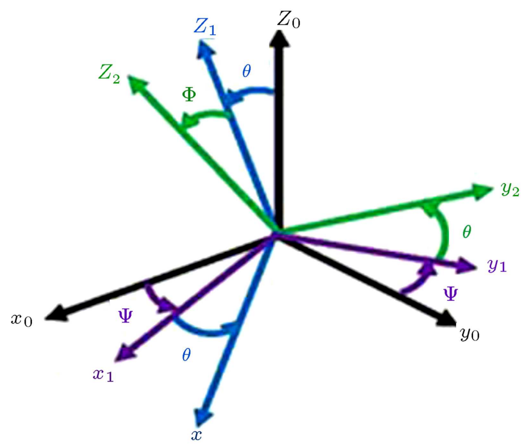

Figure 2. Transformation between inertial and rotating coordinates using Euler angles [3].

where R_ϕ and R_θ are rotational matrices about x and y, respectively. Since torsional deformations are neglected and the rotational speed of the rotor is constant, the magnitude of $\dot{\psi}$ is equal to the rotational rotor speed Ω.

By solving Eq. (1), angular velocities ω_x, ω_y, and ω_z are determined as follows:

$$\begin{bmatrix} \omega_x \\ \omega_y \\ \omega_z \end{bmatrix} = \begin{bmatrix} \dot{\phi} - \Omega\theta \\ \dot{\theta} + \Omega\phi \\ \Omega(1 - \frac{\theta^2}{2} + \frac{\phi^2}{2}) - \dot{\theta}\phi \end{bmatrix}. \quad (2)$$

For this asymmetric rotating shaft, which is modeled by the Timoshenko beam, kinetic and potential energies are derived in the rotating coordinate system in order to have a constant mass moment of inertia about x and y axes during the rotation.

The kinetic energy of the rotor consists of rotational and translational kinetic energies for the shaft and the disk:

$$T_{Rotor} = T_{Ro\_S} + T_{Ro\_D} + T_{Tr\_S} + T_{Tr\_D}. \quad (3)$$

The rotational kinetic energy of the rotor can be determined as follows:

$$T_{Ro\_S} = \frac{1}{2} \int_0^{L_2} \left(J_{tx}{\omega_x}^2 + J_{ty}{\omega_y}^2 + J_p{\omega_z}^2 \right) dz. \quad (4)$$

Also, the rotational kinetic energy of the shaft and disk of this rotor using Eq. (2) is equal to:

$$T_{Ro\_S} = \frac{\rho I}{2} \int_0^{L_2} \{ \dot{\phi}^2 + \dot{\theta}^2 - \Omega^2(\phi^2 + \theta^2) + 2\Omega^2$$

$$-2\Omega(\theta\dot{\phi} + \dot{\theta}\phi) \} dz +$$

$$\frac{\rho\Delta I}{2}\int_0^L\left\{\left(\dot\phi^2-\dot\theta^2\right)+\Omega^2(-\phi^2+\theta^2)\right.$$
$$\left.-2\Omega(\theta\dot\phi+\dot\theta\phi)\right\}dz, \tag{5}$$

$$T_{Ro\_D}=\frac{1}{2}J_{tD}\left(\dot\phi^2+\dot\theta^2\right)-J_{tD}\Omega(\phi\dot\theta+\dot\phi\theta)$$
$$-\frac{1}{2}J_{tD}\Omega^2\left(\phi^2+\theta^2\right), \tag{6}$$

where $I=\frac{I_x+I_y}{2}$, $\Delta I=\frac{I_y+I_x}{2}$, I_x, and I_y are the moments of inertia about x and y axes, respectively.

The translational kinetic energy of the rotor can be determined as follows:

$$T_{Tr}=\frac{1}{2}\int_0^{L_2}\rho A\left({V_1}^2+{V_2}^2+{V_3}^2\right)dz. \tag{7}$$

Deformation vectors are determined as follows [3]:

$$\begin{bmatrix} u_p(z,t)\\ v_p(z,t)\\ w_p(z,t)\end{bmatrix}=\begin{bmatrix} u(z,t)\\ v(z,t)\\ w(z,t)\end{bmatrix}+\begin{bmatrix}\cos\theta & 0 & \sin\theta\\ 0 & 1 & 0\\ -\sin\theta & 0 & \cos\theta\end{bmatrix}$$
$$\begin{bmatrix}1 & 0 & 0\\ 0 & \cos\phi & -\sin\phi\\ 0 & \sin\phi & \cos\phi\end{bmatrix}\begin{bmatrix}e_x\\ e_y\\ 0\end{bmatrix}, \tag{8}$$

where $\begin{bmatrix} u(z,t)+e_x\\ v(z,t)+e_y\\ w(z,t)\end{bmatrix}$ is the position of the mass center of the disk considering mass eccentricity distribution with respect to x, y, and z, respectively, and $\begin{bmatrix} u_p(z,t)\\ v_p(z,t)\\ w_p(z,t)\end{bmatrix}$ is the position of the mass center of the disk in x_1, y_1, and z_0 coordinate system, as shown in Figure 2, and is called the rotating coordinate system. Translational velocities in the rotational coordinates can be determined as follows:

$$\begin{bmatrix}V_1\\ V_2\\ V_3\end{bmatrix}=\begin{bmatrix}\dot u_p\\ \dot v_p\\ \dot w_p\end{bmatrix}+\Omega(\vec{k}).\begin{bmatrix}u_p(\vec{i})\\ v_p(\vec{j})\\ w_p(\vec{k})\end{bmatrix}. \tag{9}$$

Therefore, translational kinetic energy for this rotor is equal to:

$$T_{Tr\_s}=\int_0^{L_2}\frac{1}{2}\mu_s[\dot u^2+\dot v^2+\Omega^2(u^2+v^2)$$
$$+2\Omega(u\dot v-\dot u v)]dz, \tag{10}$$

$$T_{Tr\_D}=\frac{1}{2}M_D[\dot u^2+\dot v^2+\Omega^2(u^2+v^2)$$
$$+2\Omega(u\dot v-\dot u v)]_{z=L_1}+M_D[\Omega^2(v\varepsilon_y+u\varepsilon_x)$$
$$-\Omega(\dot u\varepsilon_y-\dot v\varepsilon_x)], \tag{11}$$

where $\mu_s=\rho A$.

Considering Timoshenko model, the strain energy for the shaft of this rotor can be obtained:

$$U_s=\frac{1}{2}\int_0^{L_2}\left[KGA\left(\frac{\partial u}{\partial z}-\theta\right)^2+KGA\left(\frac{\partial v}{\partial z}+\phi\right)^2\right.$$
$$\left.+E(I-\Delta I)(\frac{\partial\phi}{\partial z})^2+E(I+\Delta I)(\frac{\partial\theta}{\partial z})^2\right]dz, \tag{12}$$

where E, G, and K are Young's modulus, shear modulus, and Timoshenko shear coefficient, respectively. It should be noted that the Timoshenko shear coefficient is considered 0.8 in this study.

In order to model the misalignment induced forces, the reaction forces proposed by Gibbons [4] are used in this study, and the dynamic model of misalignment induced forces according to the model introduced by Jafari and Jamshidi [23] for the inertial coordinate system is as follows:

$$F_{mis\_x}=f_{mis1}(\sin(\Omega t)+\sin(2\Omega t)),$$
$$F_{mis\_y}=f_{mis2}(\cos(\Omega t)+\cos(2\Omega t)), \tag{13}$$

where f_{mis1} and f_{mis2} are obtained according to Gibbons' equations (Appendix A).

By applying the transfer matrix to this force, the dynamic model of the misalignment forces applied in the rotating coordinate system is obtained as follows:

$$F_{mis\_r}=\begin{bmatrix}\cos\psi & \sin\psi & 0\\ -\sin\psi & \cos\psi & 0\\ 0 & 0 & 1\end{bmatrix}\begin{bmatrix}F_{mis\_x}\\ F_{mis\_y}\\ 0\end{bmatrix}. \tag{14}$$

The work done by this force is equal to:

$$W_{mis\_x}=[\cos(\Omega t)f_{mis1}(\sin(\Omega t)+\sin(2\Omega t))$$
$$+\sin(\Omega t)f_{mis2}(\cos(\Omega t)+\cos(2\Omega t))]u_{(L_2)},$$
$$W_{mis\_y}=[-\sin(\Omega t)f_{mis1}(\sin(\Omega t)+\sin(2\Omega t))$$
$$+\cos(\Omega t)f_{mis2}(\cos(\Omega t)+\cos(2\Omega t))]v_{(L_2)}. \tag{15}$$

It is worthy to note that the difference between the current findings and the results achieved by Jafari and Jamshidi [23] results from the coordinate systems used. The rotating coordinates were used in this study, while Jafari and Jamshidi utilized global coordinates.

3. Application of the Rayleigh-Ritz method and Hamilton's principle

In order to approximate the functions of $u(z,t)$ and $v(z,t)$, displacements in x and y directions, and $\theta(z,t)$ and $\phi(z,t)$ as rotational angles about y and x axes, the Rayleigh-Ritz method can be used. In this method, the functions u, v, θ, and ϕ can be expressed as follows:

$$u(z,t)=a(t)\bar{u}(z), \quad v(z,t)=b(t)\bar{v}(z),$$
$$\theta(z,t)=c(t)\bar{\theta}(z), \quad \phi(z,t)=d(t)\bar{\phi}(z), \tag{16}$$

where $a(t)$, $b(t)$, $c(t)$, and $d(t)$ are independent time functions. The chosen displacement is the exact first bending mode shape of a beam, simply supported at both ends; therefore, the shape modes can be assumed as [3]:

$$\bar{u}(z)=\bar{v}(z)=\sin\frac{\pi z}{L},$$
$$\bar{\theta}(z)=\bar{\phi}(z)=\cos\frac{\pi z}{L}. \tag{17}$$

By applying the Hamilton's principle to the kinetic and strain energies, we have:

$$\delta\int_0^t (T_{Tr\_D}+T_{Tr\_s}+T_{Ro\_D}+T_{Ro\_s}-U_s +W_{mis})dt=0. \tag{18}$$

Now, the differential equations of motion can be derived as:

$$\begin{bmatrix} M_{11} & & & \\ & M_{22} & & \\ & & M_{33} & \\ & & & M_{44} \end{bmatrix}[\ddot{r}]+\begin{bmatrix} C_{11} & & & \\ & C_{22} & & \\ & & & \\ & & & \end{bmatrix}[\dot{r}]+2\Omega\begin{bmatrix} & -G & & \\ G & & & \\ & & & \\ & & & \end{bmatrix}[\dot{r}]$$
$$+\begin{bmatrix} K_{11} & & K_{13} & \\ & K_{22} & & K_{24} \\ K_{31} & & K_{33} & \\ & K_{42} & & K_{44} \end{bmatrix}[r] +\Omega^2\begin{bmatrix} -N_{11} & & & \\ & -N_{22} & & \\ & & N_{33} & \\ & & & N_{44} \end{bmatrix}[r] =\begin{bmatrix} F_x \\ F_y \\ 0 \\ 0 \end{bmatrix}, \tag{19}$$

where $[r]=\begin{bmatrix} a \\ b \\ c \\ d \end{bmatrix}$ and the components of the matrices in Eq. (19) are as follows:

$$M_{11}=\int_0^{L_2}\mu_s\bar{u}^2_{(z)}dz+M_D\bar{u}^2_{(l_1)},$$

$$M_{22}=\int_0^{L_2}\mu_s\bar{v}^2_{(z)}dz+M_D\bar{v}^2_{(L_1)}$$

$$M_{33}=\int_0^{L_2}\rho(I-\Delta I)\bar{\theta}^2_{(z)}dz+J_{Dy}\bar{\theta}^2_{(L_1)},$$

$$M_{44}=\int_0^{L_2}\rho(I+\Delta I)\bar{\phi}^2_{(z)}dz+J_{Dx}\bar{\phi}^2_{(L_1)},$$

$$C_{11}=C_{22}=c_i,$$

$$G=\int_0^{L_2}\mu_s\bar{v}_{(z)}\bar{u}_{(z)}dz+M_D\bar{v}_{(L_1)}\bar{u}_{(L_1)},$$

$$K_{11}=-\int_0^{L_2}KGA\bar{u}''_{(z)}\bar{u}_{(z)}dz,$$

$$K_{13}=\int_0^{L_2}KGA\bar{\theta}'_{(z)}\bar{u}_{(z)}dz,$$

$$K_{22}=-\int_0^{L_2}KGA\bar{v}''_{(z)}\bar{v}_{(z)}dz,$$

$$K_{24}=-\int_0^{L_2}KGA\bar{\phi}'_{(z)}\bar{v}_{(z)}dz,$$

$$K_{31}=-\int_0^{L_2}KGA\bar{\theta}_{(z)}\bar{u}'_{(z)}dz,$$

$$K_{33}=\int_0^{L_2}(KGA\bar{\theta}^2_{(z)}-E(I+\Delta I)\bar{\theta}''_{(z)}\bar{\theta}_{(z)})dz,$$

$$K_{42}=\int_0^{L_2}KGA\bar{\phi}_{(z)}\bar{v}'_{(z)}dz,$$

$$K_{44}=\int_0^{L_2}(KGA\bar{\phi}^2_{(z)}-E(I-\Delta I)\bar{\phi}''_{(z)}\bar{\phi}_{(z)})dz,$$

$$N_{11}=\int_0^{L_2}\mu_s\bar{u}^2_{(z)}dz+M_D\bar{u}^2_{(L_1)},$$

$$N_{22}=\int_0^{L_2}\mu_s\bar{v}^2_{(z)}dz+M_D\bar{v}^2_{(L_1)},$$

$$N_{33}=\int_0^{L_2}\rho(I-\Delta I)\bar{\theta}^2_{(z)}dz+J_{tD}\bar{\theta}^2_{(L_1)},$$

$$N_{44}=\int_0^{L_2}\rho(I+\Delta I)\bar{\phi}^2_{(z)}dz+J_{tD}\bar{\phi}^2_{(L_1)},$$

$$F_x=[\cos(\Omega t)f_{mis1}(\sin(\Omega t)+\sin(2\Omega t)) +\sin(\Omega t)f_{mis2}(\cos(\Omega t)+\cos(2\Omega t))]\bar{u}_{(l_2)} +M_D\Omega^2\varepsilon_x\bar{u}_{(l_1)},$$

$$F_y=[-\sin(\Omega t)f_{mis1}(\sin(\Omega t)+\sin(2\Omega t)) +\cos(\Omega t)f_{mis2}(\cos(\Omega t)+\cos(2\Omega t))]\bar{v}_{(l_2)} +M_D\Omega^2\varepsilon_y\bar{v}_{(l_1)}. \tag{20}$$

4. Numerical study

Two rotors with geometrical and material properties are considered, as introduced in Table 1.

By substituting the term $\bar{r}e^{st}$ in matrices in Eq. (19) with r and ignoring the excitation, the Campbell diagram is derived and shown in Figure 3. It should be noted that s is a complex number and has two parts. The real part and the imaginary part versus rotational speed are plotted separately and presented in Figures 3 and 4 for two rotors with different cross-sections.

Rotors 1 and 2 are used to compare the Timoshenko and Euler-Bernoulli beam theories for different dimensions of the shaft's cross-section, as shown in Figures 3 and 4.

In Figures 3 and 4(i), (b), four frequencies can be seen versus each rotational speed. This is due to the four variables in r in the Timoshenko beam theory, two of which will not usually appear in the response due to the small amplitude of the high-frequency response [2], while In Figures 3 and 4(d), there are only two frequencies versus rotational speed.

Due to the asymmetry of shaft, the rotor system will be unstable in a certain frequency range [23]. Figure 3(i) shows that in the rotational speed range between 1760 and 2320 (rad/s), the real part of the response consists of some positive values, meaning that the rotor is unstable in this range. On the other hand, one of the diagrams corresponding to the imaginary responses has a zero magnitude in this frequency range,

Table 1. Geometrical and material properties of rotor.

Shaft properties	$\rho = 7800$ kg/m^{-3}, $E = 200 \times 10^9$ N/m^{-2}, $c = 0.001$, $L_1 = 92$ mm, $L = 240$ mm, $L_2 = 320$ mm		
	Case 1	Cross-section's dimension	$sx = 20$ mm, $sy = 15$ mm
		Shaft thin ratio	$\frac{20}{240} = \frac{1}{12}$
	Case 2	Cross-section's deimension	$sx = 4$ mm, $sy = 6$ mm
		Shaft thin ratio	$\frac{6}{240} = \frac{1}{40}$
Disk properties	$R_2 = 150$ mm, $R_1 = 30$ mm, $h = 10$ mm, $J_{Dx} = J_{Dy} = M_D(3{R_1}^2 + 3{R_2}^2 + h^2)/12$		

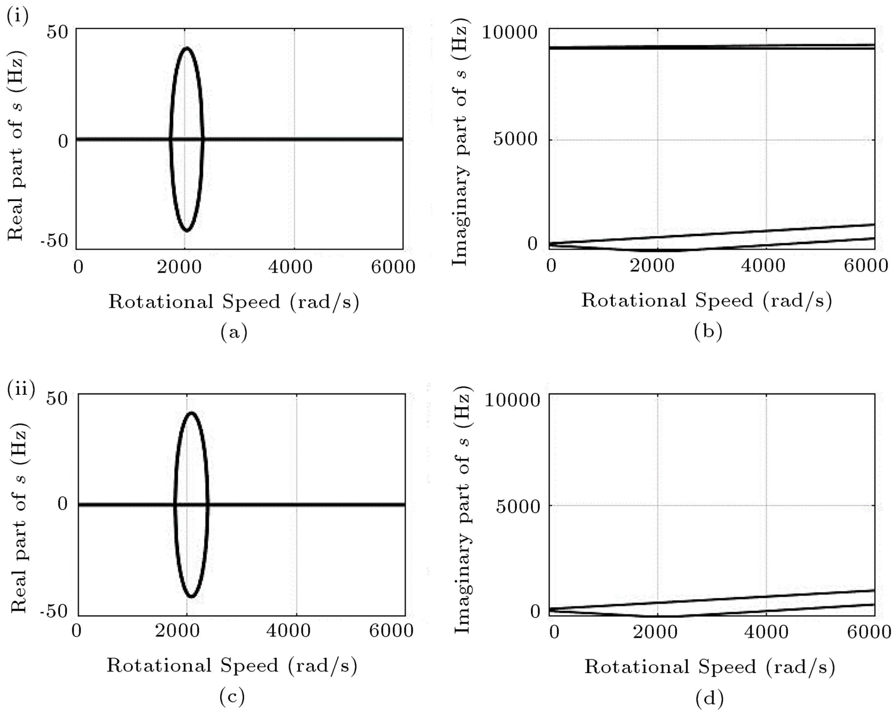

Figure 3. Campbell diagram of the rotor 1 in the rotating coordinate: (i) Timoshenko, (ii) Euler-Bernoulli beam theory: (a) and (c) real part of responses, (b) and (d) imaginary part of responses.

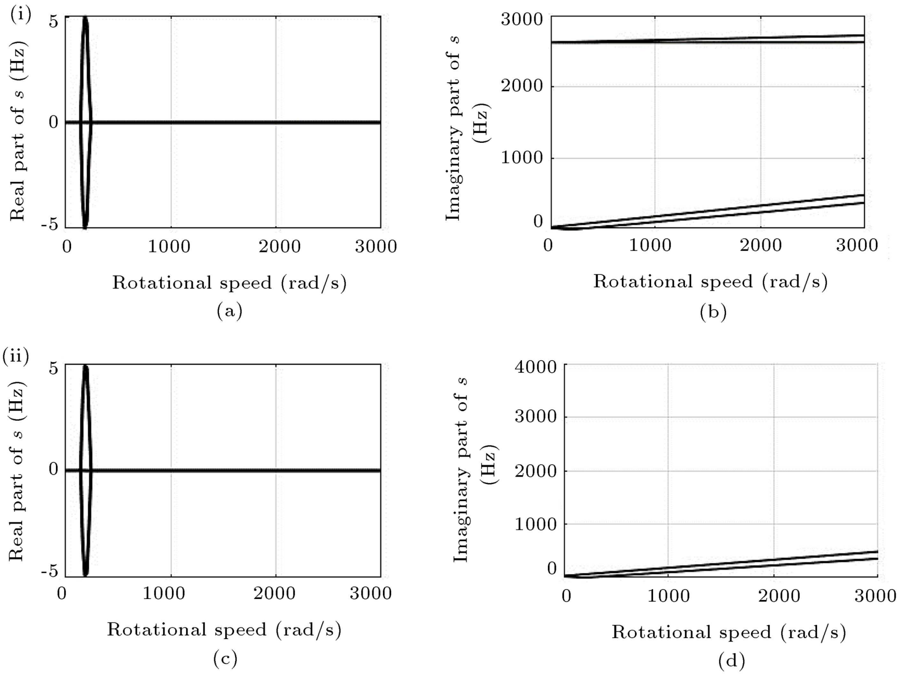

Figure 4. Campbell diagram of the rotor 2 in the rotating coordinate: (i) Timoshenko, (ii) Euler-Bernoulli beam theory: (a) and (c) real part of responses, (b) and (d) imaginary part of responses.

meaning that the resonance occurs in the system. In Figure 3(ii), this frequency for Euler-Bernoulli beam theory ranges between 1800 and 2360 (rad).

In order to investigate the effects of shaft dimensions on this frequency range, the cross-sectional area is modified in case 2, as depicted in Figure 4. both Figures 4(i) and (ii) show that in the rotational speed range between 125 and 183 (rad/s), the real part of the response consists of some positive values and also, one of the diagrams of the imaginary responses has a zero magnitude. Furthermore, according to the Ref. [23], the instability of the rotor, which has a thin shaft in case 2, starts from the rotational speed of 1477 (rpm) or 155 (rad/s). The difference between the results is less than 3.5%.

In Figure 5, high frequencies of Figure 3(b) and Figure 4(b) are neglected in order to determine the differences between the results of Timoshenko and Euler Bernoulli theories more clearly. From the results, it is clear that the Euler-Bernoulli theory responses for the rotors with larger ratios of cross-section to length are not as accurate as those of the Timoshenko theory.

5. Experimental model

The experimental setup used in this research is a model of the machinery fault simulator, shown in Figure 6. Test Rig is a rotor with the ability to install one or more discs connected via a flexible coupling to a variable drive motor. To simulate the effect of asymmetry in rotating equipment, a rectangular shaft has been designed and the shaft has been replaced with a circular cross-section to determine the effect of the rotor asymmetry in the designed experiments. The disk has the ability to install a bolt to simulate the effect of mass unbalance at different radii to determine its effect on vibrations. To investigate the parallel misalignment, the shims will be placed underneath the Bearings nos. 1 and 2, as shown in Figure 6. Leonova Diamond instrument will be used for data acquisition. MATLAB software is used for further analysis of the data acquired. The general characteristics of the device are given in Table 2. An experimental test is performed for further evaluation of rotor 2, as shown in Figure 7. In this test, mass unbalance and misalignment forces in rotor 2 are considered for finding the frequency range in which the rotor will become unstable. As shown in Figure 6, it is clearly observed that the instability zone is between 1160 and 1690 (rpm), or between 121 and 176 (rad/s), where the difference between this observed frequency range and the values obtained from Eq. (19) is less than 5%.

Also, based on the results obtained from the theoretical method, it is noted that the instability frequency range for rotor 1 begins from 1760 (rad/s) to 16815 (rpm), which can only be achieved by a powerful motor, not usually available in academic facilities. Thereafter, by solving Eq. (19), the misalignment and mass unbalance response of the rotor will be derived. The Runge-Kutta numerical method is used to solve this equation. The differential equations of motion for an aligned rotor with unbalance mass are solved

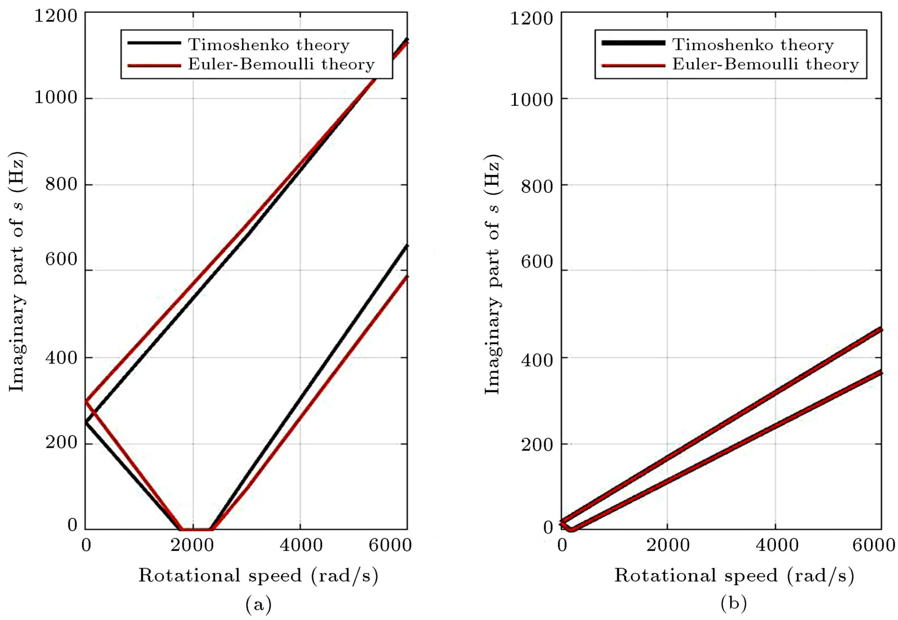

Figure 5. Comparison of Timoshenko and Euler-Bernoulli theories by plotting the imaginary part of the responses considering (a) rotor 1 and (b) rotor 2.

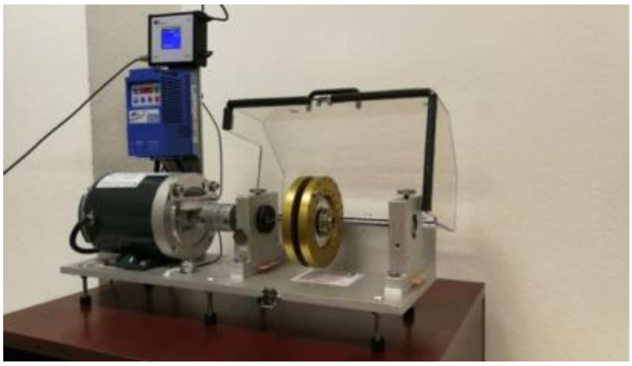

Figure 6. Machinery fault simulator.

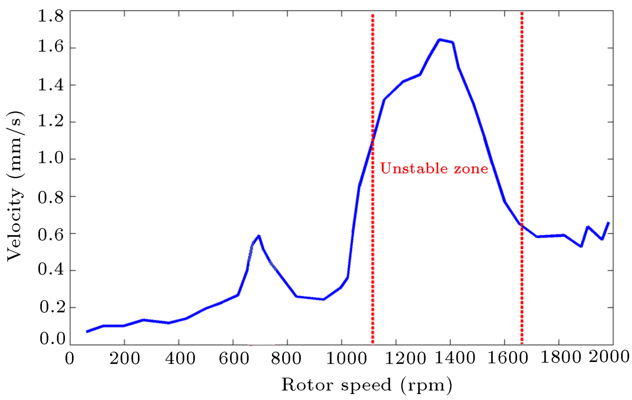

Figure 7. Experimental run-up test of rotor 2 considering misalignment and unbalance forces.

to investigate the effects of the unbalance mass; in doing so, the effects of the misalignment can be studied. As introduced in Eq. (16), a and b are independent time functions of $u(z,t)$ and $v(z,t)$ respectively. The responses of the unbalanced rotor consist of three frequencies, as shown in Figures 8 and 9, where the first one is equal to zero due to the application of the constant unbalance force. The other two frequencies result from the rotor's critical speed in the rotating coordinate at $\Omega = 3000$ (rad/s), as can be found in the imaginary plots of Figure 3(b) and (d), and the small effects of the high-frequency responses are neglected for the Timoshenko beam model. As shown in Figure 3,

Table 2. Specification of the rotor used in the test.

Rotor-bearing-pedestal feature	Value (unit)
Rotor shaft	
Shaft material	Steel
Shaft length between bearing	240 mm
Total shaft length	362 mm
Shaft no. 2 cross-section	Circle
Diameter	19.05 mm
Shaft no. 2 cross-section	Rectangular
Length and width shaft cross section	4*6 mm*mm
Density of shaft material	7800 kg/m^3
Young's modulus (E)	200 GPa
Disk	
Diameter	151 mm
Mass	0.571 kg
Thickness	10 mm
Motor	
Speed range	0–4000 rpm
Motor power rating	1.0 HP AC
Bearing no.	ER-10K

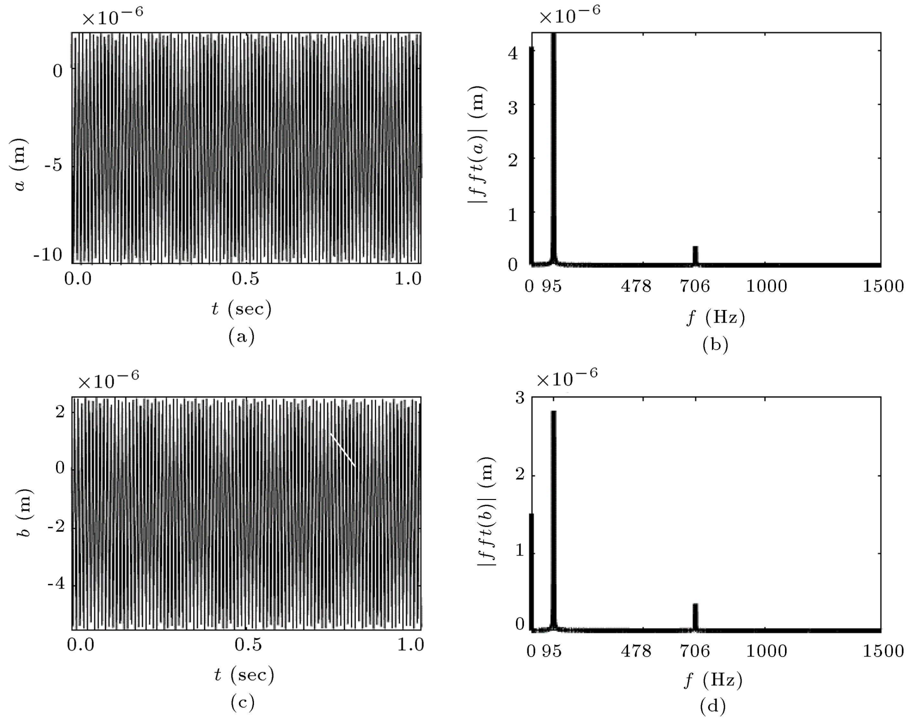

Figure 8. Unbalance vibration response of the aligned rotor 1 considering Euler-Bernoulli beam model at $\Omega = 3000$ (rad/s) or $\Omega = 478$ (Hz): (a) and (c) vibration waveforms, (b) and (d) FFT.

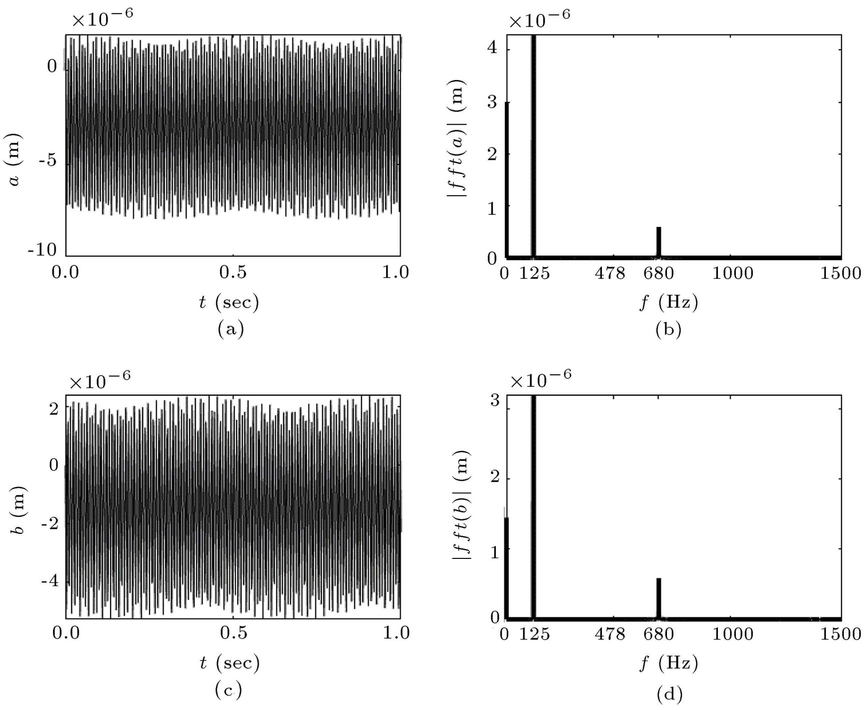

Figure 9. Unbalance vibration response of the aligned rotor 1 considering Timoshenko beam model at $\Omega = 3000$ (rad/s) or $\Omega = 478$ (Hz): (a) and (c) vibration waveforms, (b) and (d) FFT.

although the responses of the rotor in both Timoshenko and Euler-Bernoulli beam are close together, there are much less differences in the accuracy of the Timoshenko model. Given that there is not much difference in the instability frequency range between the two theories, this small difference, as shown in Figures 8 and 9, leads to a large difference in the frequency response of the system.

By solving Eq. (19) for rotor 1 and considering misalignment induced forces using the Timoshenko

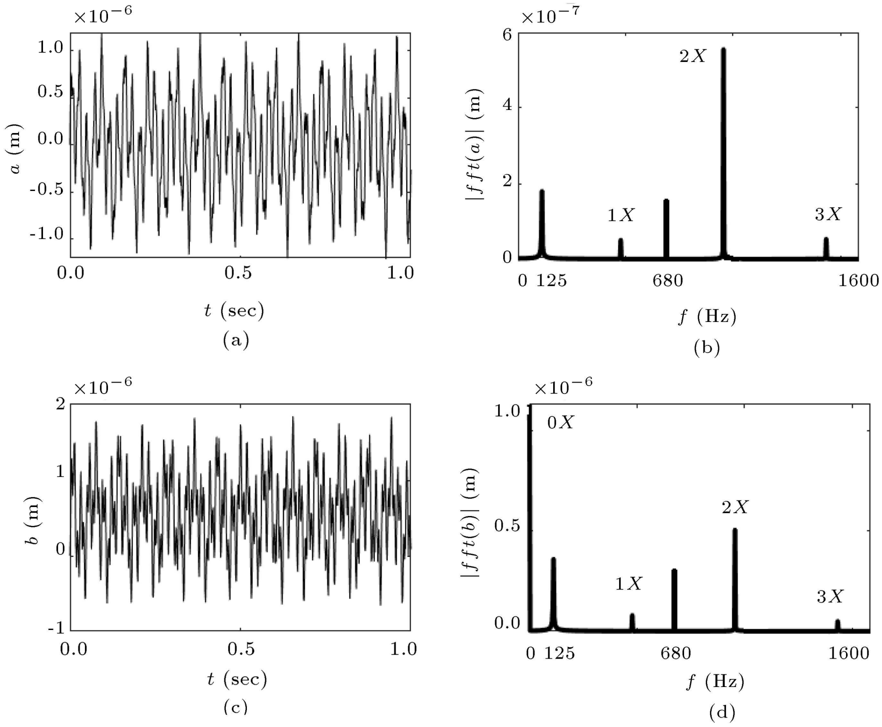

Figure 10. Vibration response of the balanced rotor 1 with the parallel misalignment considering Timoshenko beam model at $\Omega = 3000$ (rad/s) or $\Omega = 478$ (Hz): (a) and (c) vibration waveforms, (b) and (d) FFT.

model, these effects can be seen in Figure 10. The parallel misalignments $\Delta X = 0.1$ mm and $\Delta Y = 0$ mm are considered for rotor 1 at $\Omega = 3000$ (rad/s) [23].

In Figure 10, the responses include some frequencies due to the parallel misalignment. In part (b) of this figure, there is no zero frequency response unlike the part (d), and this is because of the application of the misalignment induced forces in Eq. (15). As can be observed, the response of the parallel misalignment induced forces consists of the frequencies of 1X (478 Hz), 2X (956 Hz), and 3X (1434 Hz) in the x-direction and the frequencies of 0X, 1X, 2X, 3X in the y-direction. Also, there are two critical speed frequencies of (125 Hz), (680 Hz) in both directions. The rotor orbits are plotted for the three frequencies. The first one is less than the resonance frequency; the second one is within the resonance frequency range; and the third one is higher than the range, as shown in Figures 11 and 12.

According to our findings, the vibration amplitude is acceptable when the operating speed is out of the resonance frequency range and the rotor is unstable within this range.

Figures 11(b) and 12(b) show a straight line, meaning that the rotor has a straight motion from the observer's point of view in the rotating coordinate system. In other words, at any given moment, the observer sees that the rotor gets farther and farther away from him, and as shown in the Campbell diagrams, the observer notices zero frequency in the resonance frequency range.

6. Conclusion

Although numerous studies have been performed on the asymmetric rotors, some existing research studies have not considered the Timoshenko shaft model and others have neglected the impact of misalignment forces on the dynamic behavior of the rotor. The dynamic behavior of a rotor with a rectangular shaft modeled by Timoshenko beam theory was studied in the present study under the effect of mass unbalance and misalignment induced forces in the rotating coordinates. Gibbons' equations were applied for calculating the forces due to coupling misalignment.

By plotting Campbell diagrams, this study investigated the natural frequencies of the system and found a frequency range that resulted in its instability. Also, the effects of the cross-section on this frequency range were studied considering two rotors with different cross-sections. Based on the comparison between Timoshenko and Euler-Bernoulli beam theories, it was concluded that in the case of thin shafts, both theories achieved the same results, while in the case of thick shafts, the Euler-Bernoulli beam theory did not help obtain accurate results. In this study, it was proved that using the Timoshenko's beam theory could increase the accuracy of the results, especially in case where the ratio of the cross-section to the length of

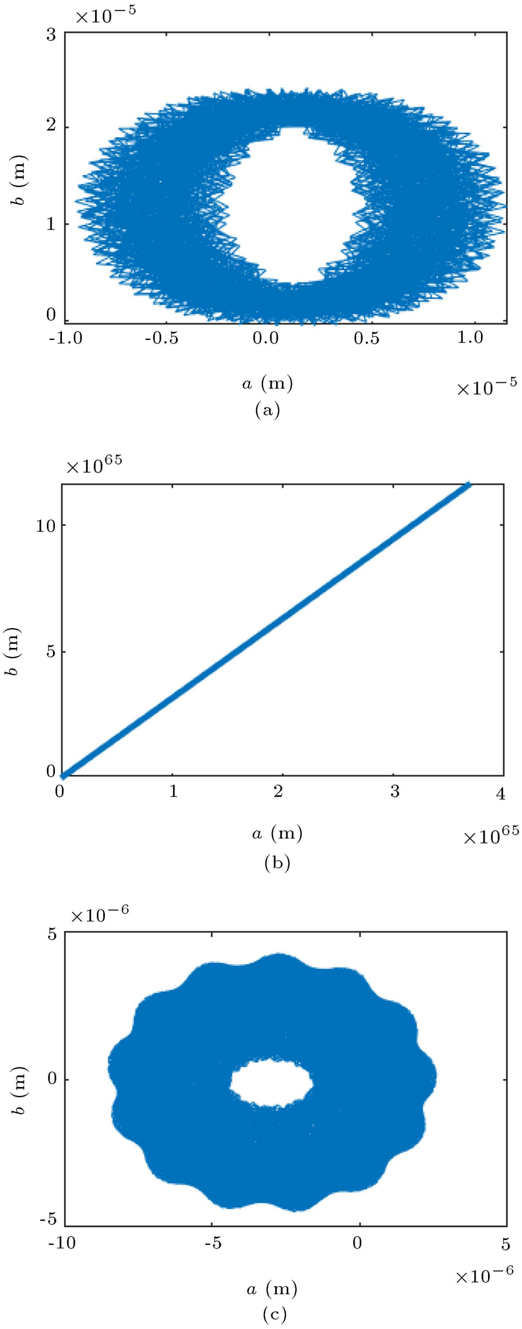

Figure 11. Orbit plot of the rotor 1 with the parallel misalignment and unbalance forces (a) $\Omega = 1500$ (rad/s) (b) $\Omega = 1800$ (rad/s) (c) $\Omega = 3000$ (rad/s).

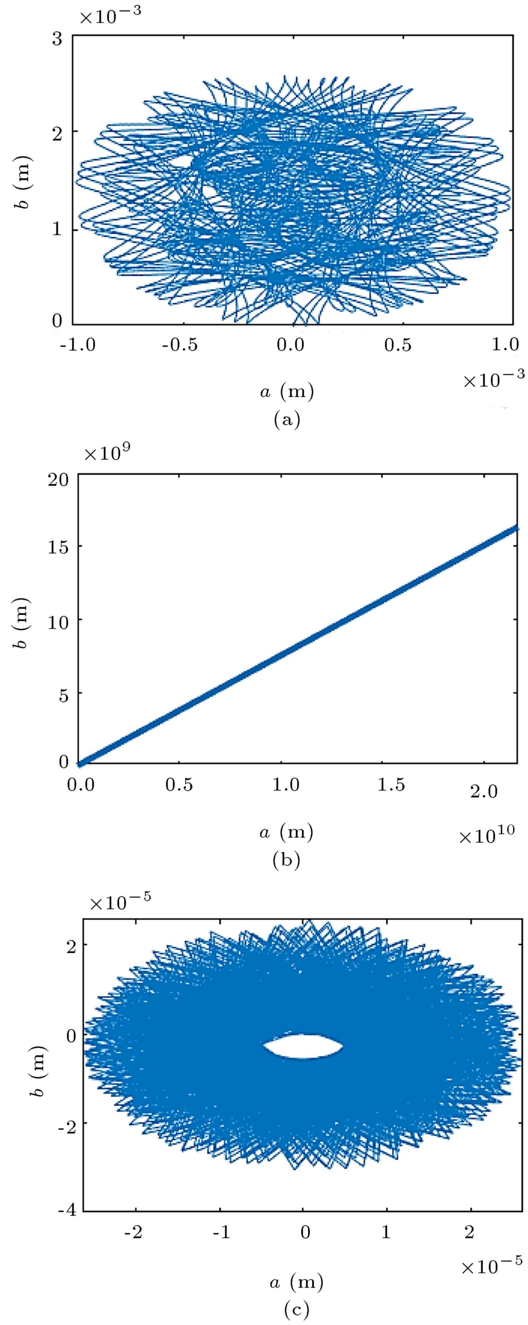

Figure 12. Orbit plots of the rotor 2 with the parallel misalignment and unbalance forces (a) $\Omega = 100$ (rad/s) (b) $\Omega = 200$ (rad/s) (c) $\Omega = 300$ (rad/s).

the shaft was larger. Thereafter, vibration waveforms of the rotors and their Fast Fourier Transforms were plotted so that the frequencies of the vibrations could specify the behavior of the rotor and identify defects in the system. It was shown that the response of the misaligned rotor consisted of the frequencies of 0X, 1X, 2X, 3X, and the response of the unbalanced rotor consisted of the frequency of 0X. Furthermore, orbit plots were figured for the rotors in three frequencies. As expected, it was shown that the vibration amplitude could be acceptable if the operating speed was out of the resonance frequency range and the rotor was unstable within this range. Therefore, the results obtained in this study clearly showed the difference between the theory of Timoshenko and Euler-Bernoulli, and also from the comparison with previous studies conducted in the inertial coordinate system, we can see the difference between the results of this study and them.

To verify the theoretical results for the model, an experimental setup was constructed to test the asymmetric rotor connected to an electric motor with misalignment. The measurements and experimental results showed that the resonance frequency range was close to what had been obtained from the Campbell diagram.

Acknowledgements

We would like to express our deep gratitude to Dr. Jamshidi, Head of Turbomachinery Maintance of the South Pars Gas Complex (SPGC), and Dr. Samsami, Faculty Member of West Tehran Branch, Islamic Azad University for their advice and assistance in keeping our progress on schedule and organizing the experimental tests. We would also like to extend our thanks to the technicians of the laboratory of the South Pars Gas Complex(SPGC) Refinery Plant Phase 2&3 CBM Department for their help in offering us the resources in running the program and using their Machinery Fault Simulator to verify our theoretical results.

Nomenclature

Ω	Angular velocity of the rotor (rad/s^{-1})
$\phi(z,t)$	Rotational angles about x Axis (m)
$\theta(z,t)$	Rotational angles about y axis (m)
$\psi(z,t)$	Rotational angles about z axis (m)
$u(z,t)$	Displacement along x-axis of rotor (m)
$v(z,t)$	Displacement along y-axis of rotor (m)
I	Average area moment of inertia of shaft (m^4)
c_i	Coefficient of damping (N/s/m^{-1})
R_1	Cross-sectional radius of shaft/internal radius of disk (m)
A	Cross-sectional area of shaft (m^2)
ρ	Density of material (kg/m^{-3})
T_{Ro_S}	Translational kinetic energy of shaft (N/m)
T_{Ro_D}	Translational kinetic energy of sisk (N/m)
T_{Tr_S}	Rotational kinetic energy of shaft (N/m)
T_{Tr_D}	Rotational kinetic energy of disk (N/m)
U_s	Strain (deformation) energy of shaft (N/m)
J_{Dx}	Mass moment of inertia of disk in direction x (kg/m^2)
J_{Dy}	Mass moment of inertia of disk in direction x (kg/m^2)
M_D	Mass of disk (kg)
e_x	Position of mass center of disk from the center of disk in direction x (m)
e_y	Position of mass center of disk from the center of disk in direction y (m)
L_1	Position of disk on shaft (m)
L	Distance between the bearings (m)
L_2	Length of the shaft (m)

References

1. Michel, F., *Rotordynamics, Prediction in Engineering*, 2nd Ed., John Wiley & Sons, Chichester, UK (1998).

2. Genta, G., *Dynamics of Rotating Systems*, Springer, New York (2005).

3. Muszynska, A. "Rotordynamics", Taylor & Francis, Broken Sound Parkway, Routledge (2005).

4. Gibbons, C.B. "Coupling misalignment forces", *Proceedings of the 5th Turbomachinery Symposium*, A&M University, Texas (1976).

5. Prabhu, B.S. "An experimental investigation on the misalignment effects in journal bearings", *Tribology Transactions*, **40.2**, pp. 235–242 (1997).

6. Ganesan, S. and Padmanabhan, C. "Modeling of parametric excitation of a flexible coupling-rotor system due to misalignment", *Proceedings of the Institution of Mechanical Engineers, Part C: Journal of Mechanical Engineering Science*, **225**(12), pp. 2907–2918 (2011).

7. Wan, Z., Jing, J.P., Meng, G., et al. "Theoretical and experimental study on the dynamic response of multidisk rotor system with flexible coupling misalignment", *Proceedings of the Institution of Mechanical Engineers, Part C: Journal of Mechanical Engineering Science*, **226**(12), pp. 2874–2886 (2012).

8. Al-Hussain, K.M. and Redmond, I. "Dynamic response of two rotors connected by rigid mechanical coupling with parallel misalignment", *Journal of Sound and Vibration*, **249**(3), pp. 483–498 (2002).

9. Al-Hussain, K.M. "Dynamic stability of two rigid rotors connected by a flexible coupling with angular misalignment", *Journal of Sound and Vibration*, **266**(2), pp. 217–234 (2003).

10. Hujare, D.P. and Karnik, M.G. "Vibration responses of parallel misalignment in Al shaft rotor bearing system with rigid coupling", *Materials Today. Proceedings*, **5.11**, pp. 23863–23871 (2018).

11. Verma, Kumar, A., Sarangi, S., and Kolekar, M.H. "Experimental investigation of misalignment effects on rotor shaft vibration and on stator current signature", *Journal of Failure Analysis and Prevention*, **14**(2), pp. 125–138 (2014).

12. Ma, H., Wang, X., Niu, H., et al. "Oil-film instability simulation in an overhung rotor system with flexible coupling misalignment", *Archive of Applied Mechanics*, **85**(7), pp. 893–907 (2015).

13. Jalan, A.K. and Mohanty, A.R. "Model based fault diagnosis of a rotor-bearing system for misalignment and unbalance under steady-state condition", *Journal of Sound and Vibration*, **327**(3–5), pp. 604–622 (2009).

14. Sudhakar, G.N. and Sekhar, A.S. "Coupling misalignment in rotating machines modeling, effects and monitoring", *Noise & Vibration Worldwide*, **40**(1), pp. 17–39 (2009).

15. Wang, N. and Jiang, D. "Vibration response characteristics of a dual-rotor with unbalance-misalignment coupling faults", *Theoretical Analysis and Experimental Study; Mechanism and Machine Theory*, **125**, pp. 207–219 (2018).

16. Gao, S, Xiong, X., Zhou, C., et al. "Dynamic behavior of a rotor-bearing system with integral squeeze film damper and coupling misalignment", In *2018 Prognostics and System Health Management Conference (PHM-Chongqing)*, IEEE, pp. 1255–1262 (2018).

17. Wang, H. and Gong, J. "Dynamic analysis of coupling misalignment and unbalance coupled faults", *Journal of Low Frequency Noise, Vibration and Active Control*, **38**(2), pp. 363–376 (2019).

18. Tondl, A. "Some problems of rotor dynamics", *LTD Translation, Chapmanand Hall*, London, p. 434 (1965).

19. Badlani, M. and Kleinhenz Wand Hsiao, C.C. "The effect of rotary inertia and shear deformation on the parametric stability of unsymmetric shafts", *Mechanism and Machine Theory*, **13**(5), pp. 543–553 (1978).

20. Srinath, R., Sarkar, A., and Sekhar. A.S. "Instability of asymmetric shaft system", *Journal of Sound and Vibration*, **362**, pp. 276–291 (2016).

21. Hili, M., Attia, M., Bouaziz, S., et al. "Stability analysis and dynamic behavior of a flexible asymmetric rotor supported by active magnetic bearings", **55**(3), pp. 751–763 (2017).

22. Raffa, F.A. and Vatta, F. "Differential equations of motion of an asymmetric Timoshenko shaft", *Meccanica*, **36**(2), pp. 201–211 (2001).

23. Jafari, A.A. and Jamshidi, P. "Investigation on linear vibration behavior of rotors with asymmetry shaft considering misalignment", *Journal of Solid Mechanics*, **11**(3), pp. 535–549 (2019).

24. Shahgholi, M. and Khadem, S.E. "Stability analysis of a nonlinear rotating asymmetrical shaft near the resonances", *Nonlinear Dynamics*, **70**(2), pp. 1311–1325 (2012).

25. Feng, S., Geng, H.P., Qi, S.M., et al. "Vibration of a misaligned rotor system with asymmetric shaft stiffness", In *Advanced Materials Research Trans Tech Publications*, **503–504**, pp. 813–818 (2012).

26. Li., Z., Li., J., and Li, M. "Nonlinear dynamics of unsymmetrical rotor-bearing system with fault of parallel misalignment", *Advances in Mechanical Engineering*, **10**(5) (2018).

27. Rahi, A. "Size effect investigation on lateral vibrations of a micro drill subjected to an axial load using the modified couple stress theory" *Scientia Iranica*, **26**(4), pp. 2441–2453 (2019).

28. Farshidianfar, A. and Soheyli, S. "Effects of rotary inertia and gyroscopic momentum on the flexural vibration of rotating shafts using hybrid modeling", *Scientia Iranica*, **16**(1), pp. 75–86 (2009).

29. Wang, Z. and Zhu, C. "A new model for analyzing the vibration behaviors of rotor-bearing system", *Communications in Nonlinear Science and Numerical Simulation*, **83**, 105130 (2020).

30. Filippi, M. and Carrera, E. "Stability and Transient Analyses of Asymmetric rotors on anisotropic supports", *Journal of Sound and Vibration*, **500**, 116006 (2021).

31. Jamshidi, H. and Jafari, A.A. "Predicting unbalance asymmetric rotor vibration behavior based on sensitivity analysis and using response surface methodology method considering parallel misalignment", *Proceedings of the Institution of Mechanical Engineers, Part C: Journal of Mechanical Engineering Science*, **235**(24), pp. 7430–7444 (2021).

32. Jamshidi, P. and Jafari, A.A. "Analytical investigation on nonlinear vibration behavior of an unbalanced asymmetric rotor using the method of multiple scales", *Journal of the Brazilian Society of Mechanical Sciences and Engineering*, **41**, Article number: 456 (2019).

33. Bab, S., Khadem, S.E., Abbasi, A., et al. "Dynamic stability and nonlinear vibration analysis of a rotor system with flexible/rigid blades", *Mechanism and Machine Theory*, **105**, pp. 633–653 (2016).

34. Lu, J., Zhang, X., Pan, X., et al. "Research on unbalanced vibration suppression method for coupled cantilever dual-rotor system", *Machines*, **10**(9), p. 758 (2022).

Appendix A

Misalignment in rotating machinery causes reaction forces and moments to be generated in the coupling as shown in Figure A.1. The forces and moments for the coupling are provided in Appendix A [4].

Reaction forces and moments for parallel misalignment:

$$MX1=Tq\sin\theta_1+K_b\phi_1, \qquad MX2=Tq\sin\theta_2-K_b\phi_2$$
$$MY1=Tq\sin\phi_1-K_b\theta_1, \qquad MY2=Tq\sin\phi_2+K_b\theta_2$$
$$FX1=(-MY1-MY2)/Z3,$$
$$FY1=(MX1+MX2)/Z3,$$

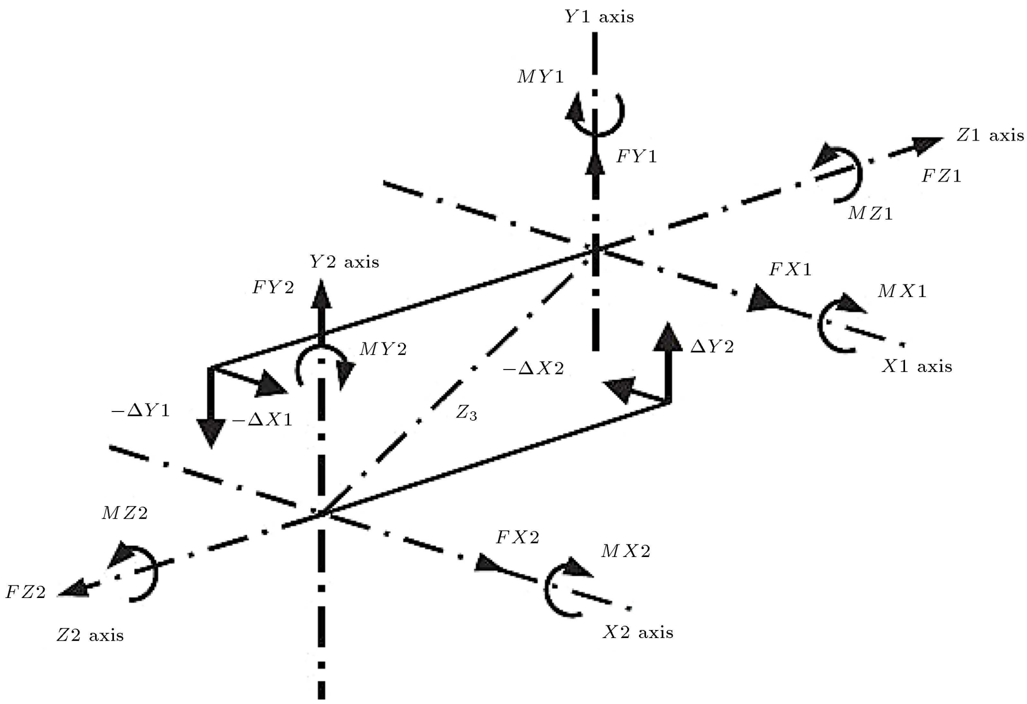

Figure A.1. Coupling coordinates system.

where:

$$\begin{cases} \theta_1 = \mathrm{Arcsin}(\Delta X1/Z3), & \theta_2 = \mathrm{Arcsin}(\Delta X2/Z3) \\ \phi_1 = \mathrm{Arcsin}(\Delta Y1/Z3), & \phi_2 = \mathrm{Arcsin}(\Delta Y2/Z3) \end{cases}$$

Biographies

Hamed Jamshidi graduated from Alborz High School. He completed his undergraduate studies in Mechanical Engineering at KNTU (Khajeh Nasir Toosi University of Technology), one of the top technical universities in Iran. He excelled in his academic pursuits and achieved the first rank among nearly 25,000 applicants for Azad University's MSc entrance exam. He also ranked 10th in the MSc National Entrance Exam in the field of Solid Design and 2nd in the field of Fluid Mechanics. In addition, he earned the 7th rank in the Olympiad of Mechanical Engineering in Iran. Due to his passion for Mechanics of Materials, he pursued a graduate degree in Mechanical Engineering specializing in Solid Design at Sharif University of Technology, the best university in Iran. He once again achieved the first rank in the Azad University entrance exam and proceeded to earn a PhD at Azad University's west Tehran branch. He has been a faculty member of Azad University's Parand branch for 16 years, teaching courses in Statics and Mechanics of Materials.

Ali Asghar Jafari graduated from Alborz High School and received his undergraduate degree in Mechanical Engineering from Sharif University of Technology, the top university in Iran. He pursued his PhD in Mechanical Engineering in Australia. As a faculty member of Khajeh Nasir Toosi University of Technology (KNTU), he taught Vibrations for 30 years and has over 70 ISI papers. He has had the honor of teaching many faculty members in Iranian universities.

Pouya Jamshidi graduated from Alborz High School and received his undergraduate degree in Mechanical Engineering from Esfahan University of Technology. He took both Azad University and National Entrance exams for his MSc studies and achieved the third rank for Azad University. He continued his studies in Mechanical Engineering at KNTU, where he ranked 14th in the entrance exam for his PhD studies. He has been the Head of Turbo Compressor Maintenance Department at SPGC for 17 years.